Contrib Mineral Petrol (2008) 155:689–702
DOI 10.1007/s00410-007-0265-x

ORIGINAL PAPER

# Transport properties of low-sanidine single-crystals, glasses and melts at high temperature

**Maik Pertermann · Alan G. Whittington · Anne M. Hofmeister · Frank J. Spera · John Zayak**

Received: 3 May 2007 / Accepted: 5 November 2007 / Published online: 27 November 2007


**Abstract** Thermal diffusivity ($D$) was measured using laser-flash analysis from oriented single-crystal low-sanidine ($K_{0.92}Na_{0.08}Al_{0.99}Fe^{3+}_{0.005}Si_{2.95}O_8$), and three glasses near $KAlSi_3O_8$. Viscosity measurements of the three supercooled liquids, in the range $10^{6.8}$ to $10^{12.3}$ Pa s, confirm near-Arrhenian behavior, varying subtly with composition. For crystal and glass, $D$ decreases with $T$, approaching a constant near 1,000 K: $D_{sat} \sim 0.65 \pm 0.3$ mm$^2$ s$^{-1}$ for bulk crystal and $\sim 0.53 \pm 0.03$ mm$^2$ s$^{-1}$ for the glass. A rapid decrease near 1,400 K is consistent with crossing the glass transition. Melt behavior is approximated by $D = 0.475 \pm 0.01$ mm$^2$ s$^{-1}$. Thermal conductivity ($k_{lat}$) of glass, calculated using previous heat capacity ($C_P$) and new density data, increases with $T$ because $C_P$ strongly increases with $T$. For melt, $k_{lat}$ reaches a plateau near 1.45 W m$^{-1}$ K$^{-1}$, and is always below $k_{lat}$ of the crystal. Melting of potassium feldspars impedes heat transport, providing positive thermal feedback that may promote further melting in continental crust.

Communicated by: T.L. Grove.

M. Pertermann
Department of Earth Science, Rice University, Houston, TX 77005, USA

A. G. Whittington
Department of Geological Sciences, University of Missouri, Columbia, MO, USA

A. M. Hofmeister (✉)
Department of Earth and Planetary Sciences, Washington University, St. Louis, MO 63130, USA
e-mail: Hofmeist@wustl.edu

F. J. Spera · J. Zayak
Department of Earth Sciences, University of California, Santa Barbara, CA 93106, USA

**Keywords** Laser-flash analysis · High temperature · Thermal diffusivity · Viscosity · Density · IR spectroscopy · Low sanidine · Single-crystal · Glass · Melt

## Introduction

Heat transport properties of minerals are needed to understand Earth's thermal state and evolution. Most measurements involve physical contact of samples with thermocouples and/or heaters (e.g., Osako et al. 2004; Höfer and Schilling 2002), despite likely problems with thermal losses at contacts (e.g. Fried 1969; Lee and Hasselman 1985) and radiative transfer (e.g., Lee and Kingery 1960). Recent advances in contact-free, laser-flash analysis (LFA) regarding use of coatings (Degiovanni et al. 1994) and mathematical models of the raw data (Mehling et al. 1998) permit complete removal of direct radiative transfer effects at geologically relevant temperatures, thereby isolating the lattice (phonon) component of thermal diffusivity ($D$). Through detailed comparison, Hofmeister (2007a, b) and Hofmeister et al. (2007) confirmed that results from contact methods are systematically altered in opposite directions and to various degrees by thermal interface resistance and spurious radiative transfer. Both $D$ and thermal conductivity,

$$k_{lat} = \rho C_P D, \quad (1)$$

where $C_P$ is heat capacity and $\rho$ is density, are affected. The subscript emphasizes that the lattice (phonon) component is our interest here. In addition, the use of cylinders with high length to diameter ratios alter the measured anisotropy from the true values due to the different manner in which transverse optic (TO) and longitudinal optic (LO)

modes couple with diffusing phonons (Hofmeister 2007a; Hofmeister et al. 2007). LFA of thin samples avoids the above problems.

So far, LFA studies have focused on materials relevant to oceanic crust and upper mantle (Hofmeister 2006, 2007a, b; Pertermann and Hofmeister 2006). However, continental crust contains different types of minerals. Feldspars are particularly important constituents, and the available high-$T$ data (Höfer and Schilling 2002) were gathered using problematic contact methods. Similarly, data on glasses, which serve as proxies for melt properties, have been collected using contact methods. Because glasses have minimal imperfections that scatter light, and are generally colorless or pale, spurious radiative transfer is likely in these experiments. Given the experimental difficulties, it should come as no surprise that controversy exists as to values for $D$ and/or $k$ of melts (cf., Bagdassarov and Dingwell 1994; Snyder et al. 1994). Resolution of this controversy requires a method that eliminates contact effects and the effects of radiative heat transport. The purpose of this work is to address this problem explicitly.

We present new thermal diffusivity data obtained using laser-flash analysis up to 1,250 K for orientated, natural gem-like, low-sanidine single-crystals and up to 1,650 K for three synthetic glasses with compositions near $KAlSi_3O_8$. Thermal conductivity is calculated from these data. The results are interpreted based on our data for the viscosity of feldspathic melts. Both $D$ and $k_{lat}$ of glass are lower than those of the analogous bulk crystal, and decrease further upon crossing the glass transition. At high $T$, $k_{lat}$ and $D$ for each phase (crystal, glass, or melt) are independent, or nearly so, of $T$. Implications of this asymptotic behavior for thermal transport in continental crust are briefly discussed.

## Experimental methods

### Synthesis procedures

Synthetic $KAlSi_3O_8$ glass "W" was prepared by grinding $SiO_2$, $Al_2O_3$, and $K_2CO_3$ powders under acetone, then heating it slowly in a platinum crucible to 1,650°C, driving off $CO_2$ in the process. The liquid was quenched, ground under acetone, and fused again two more times to ensure homogeneity. Final fusion over 72 h at 1,650°C allowed air bubbles to escape. The liquid was quenched rapidly by immersing the base of the crucible in water.

Synthetic glass "S" was prepared from reagent quality silica, alumina, and potassium carbonate heated in Pt crucibles at 1 bar and 1,635°C for 12 h. The quenched liquid was then ground, pressed and melted to remove bubbles and obtain homogeneity. Final fusion at 1,620°C lasted 50 h. Quenching is as described above.

Glass "M" was prepared by melting the crystal: several grams were wrapped in Pt foil and heated from room temperature to 1,600°C in a muffle furnace at 5°C per minute. The melt was held at 1,600°C for 190 h, then cooled at 5°C per minute to room temperature.

### Sample preparation

Samples were cut, ground, and polished into finished slabs of 8–14 mm diameter with thicknesses $\leq$1.1 mm and nearly parallel surfaces. Surfaces with a large number of bubbles were avoided. After spectroscopic and electron microprobe measurements, samples were thinned and sandblasted with alumina grit of 50–150 μm. Graphite coating was sprayed on as $\sim$4 thin layers on each surface. Total coating thicknesses of $\sim$1 μm negligibly affect $D$ for millimeter-sized samples.

For parallel plate viscosity measurements, cylindrical samples were cored from glass lumps using a diamond core drill. The cylinders were cut to lengths of 3 to 7 mm using a diamond wafer saw, polished on successively finer grit papers, and parallel faces were verified by length measurement with a micrometer.

### Electron microprobe analysis

Samples were characterized chemically by wavelength dispersive analysis (WDS) using standard procedures on the JEOL-733 and JXA-8200 electron microprobes at Washington University, using "Probe for Windows" for data reduction. Oxide and silicate standards (e.g. potassium feldspar for K, Al and Si; albite for Na; and ilmenite for Mg, Ti, and Fe) were used for calibration. Formulae were calculated on the basis of eight oxygens from the data in Table 1.

### Near-IR spectroscopy and analysis of water contents

We used an evacuated Bomem DA3.02 Fourier transform interferometer with an SiC source, an InSb detector, and a $CaF_2$ beamsplitter. Instrumental accuracy is 0.01 $cm^{-1}$. About 2,000 scans were collected at room temperature from $\sim$1,200 to 5,000 $cm^{-1}$ at a resolution of 4 $cm^{-1}$. Segments were merged and absorbance ($a$) is calculated from:

$$a = -\log(I_{trans}/I_0). \quad (2)$$

For high-silica glasses, water contents are determined from:

**Table 1** Chemical compositions (in wt%)

| | OMT crystal | OFD crystal | O glass | S glass | W glass | $KAlSi_3O_8$ |
|---|---|---|---|---|---|---|
| *n* | 2 | 6 | 2 | 7 | 11 | – |
| $SiO_2$ | 65.9 (1) | 64.64 (31) | 67.36 (15) | 64.37 (1.15) | 63.05 (51) | 64.76 |
| $TiO_2$ | 0.04 (1) | 0.02 (3) | 0.02 (1) | bld | 0.03 (3) | – |
| $Al_2O_3$ | 17.64 (3) | 18.32 (9) | 18.41 (1) | 17.69 (13) | 19.09 (10) | 18.32 |
| FeO | 1.09 (1) | 0.11 (5) | 0.45 (2) | bld | 0.05 (3) | – |
| MnO | bld | 0.01 (2) | bld | 0.02 (2) | bld | – |
| MgO | 0.01 (1) | bld | bld | bld | 0.04 (1) | – |
| CaO | 0.01 (1) | 0.01 (1) | 0.02 (1) | bld | 0.04 (1) | – |
| $Na_2O$ | 0.59 (1) | 0.91 (2) | 1.00 (1) | 0.03 (2) | 0.05 (2) | – |
| $K_2O$ | 16.20 (3) | 15.73 (10) | 14.20 (7) | 17.42 (13) | 16.68 (21) | 16.92 |
| Sum | 100.49 (5) | 99.76 (36) | 101.47 (7) | 99.53 (1.25) | 99.03 (50) | 100.00 |

$$H_2O\,wt\% = 1,802\,a/(\rho\varepsilon L), \quad (3)$$

where $\varepsilon$ = 75 L mol$^{-1}$ cm$^{-2}$, $\rho$ has units of g L$^{-1}$ and thickness $L$ has units of cm (Okamura et al. 2003). For orthoclase glass, $\rho$ = 2,360 g L$^{-1}$. Because it is not always clear whether a phase has $OH^-$ or structurally bound $H_2O$ molecules, these two species are not differentiated, and concentrations ($X$) are reported in terms of wt% $H_2O$. Relative concentrations among our samples are highly accurate, but absolute concentrations could vary by ~10% from our results.

## Viscometric measurements

Viscosity of samples W, O, and S were measured using a Theta Instruments Rheotronic III parallel plate viscometer, with a constant uniaxial load of 1,500 g, and a maximum temperature of 1,000°C. Viscosity is calculated from the measured longitudinal strain rate, known load and calculated instantaneous surface area, assuming perfect slip between sample and plates. Relatively low finite strains were used (≤20%), and samples remained cylindrical after measurement. For $KAlSi_3O_8$ glasses, measurement temperatures ranged from 928 to 982°C, with strain rates between 7 × 10$^{-8}$ and 3 × 10$^{-6}$ s$^{-1}$. The accuracy and precision of the measurements are ±0.06 log units. See Getson and Whittington (2007) for details.

Viscosity of sample S was determined by concentric cylinder rheometry. The basic measurement is of the torque exerted on the inner cylinder immersed in liquid residing in the outer cup that can be rotated at a steady rate known to about 1 part in 10$^5$. The torque data are used with the depth of immersion and cylinder radii to compute the shear viscosity. Measurements were made over a range of shear rates of about 100; over this range the liquid behaved as a Newtonian fluid with a linear relationship between shear stress and shear rate. Measurement temperatures ranged from 1,000–1,200°C. The uncertainty on viscosity as determined by running NBS standards is about ±0.05 $\log_{10}$ units. Temperatures are known to ±3 K (see Stein and Spera 1994, 1998, 2001, for details).

## Density determinations

Glass density was obtained before and after viscosity measurements using the Archimedean method, with distilled water as the immersion liquid. Repeat measurements indicate precision is typically ±1 kg m$^{-3}$ or better. Samples of S glass increased in density by ~0.8% during parallel plate viscometry, probably due to compaction of bubbles. Such a small bubble fraction (<1 volume%) should not significantly affect the viscosity results. The density of W and O glasses was the same before and after viscometry measurements.

## Thermal diffusivity measurements

Our LFA 427 apparatus is manufactured by Netzsch Gerätebau, Germany. Specimens are suspended in a graphite holder that allow analysis of a circular area with a diameter of 6–10 mm. The sample is located in the hot-spot zone of a vertical furnace and the temperature dependence of $D$ is obtained by varying furnace temperature. A single pulse from an Nd–GGG laser heats the sample from below and as heat diffuses from the bottom to the top of the sample, emissions are monitored by an InSb detector mounted above the sample. Data were acquired as time-temperature curves (Fig. 1). Temperature was measured using calibrated W–Re thermocouples, one of which is located adjacent to the sample. Data were acquired in an Ar gas atmosphere. Graphite coatings on the sample (needed to

block laser light and to enhance absorption of the pulse as well as sample emissions) buffer the oxygen fugacity at high temperatures to C–CO. Thermal diffusivity values are accurate to 2%, as verified against opaque and soft standard reference materials (graphite and Fe-alloys). Uncertainty in *D* arises largely from that of sample thickness. For details and calibration procedures, see Blumm and Lemarchand (2002), Hofmeister (2006), and Pertermann and Hofmeister (2006).

Data were obtained at 50–100°C intervals with several acquisitions at each temperature, and processed with proprietary Netzsch software, using the algorithm of Mehling et al. (1998) to extract thermal diffusivity from the time–temperature curves (Fig. 1). This accounts for both radiative surface losses to the surroundings and spurious radiative transfer through the sample between the top and bottom graphite coats, and allows for absorbance being frequency dependent, although the detailed values of optical properties are not needed. The software accounts for the measured shape of the laser pulse (Blumm and Opfermann 2002).

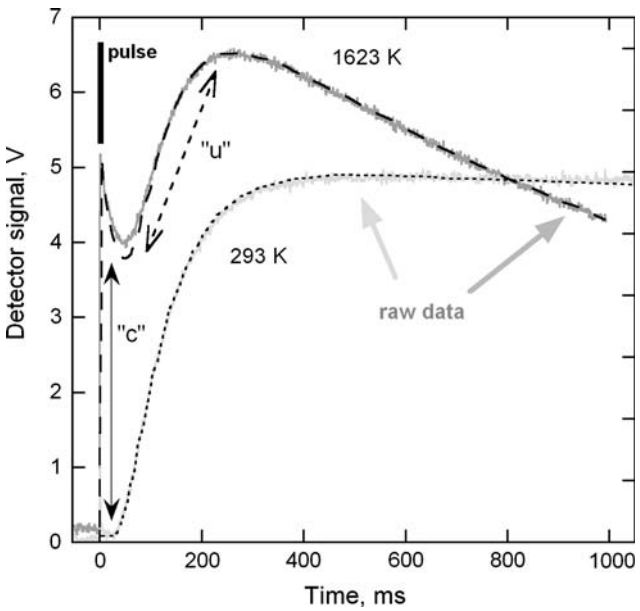


**Fig. 1** Time–temperature curves for orthoclase glass, sample S with $L = 0.71$ mm. *Broken lines* model fits. *Thick vertical line* laser pulse. *Light gray* room temperature raw data showing scant radiative transfer. After reaching maximum temperature, emissions decrease as the sample re-equilibrates. *Dark gray* raw data at the highest temperatures reached, with a large amount of radiative transfer (*double arrow* marked "c") immediately after the laser pulse. Slow phonon travel occurs gradually after the laser pulse, indicated by the *dotted double arrow* marked "u"

## Sample descriptions, composition, structure, and water contents

Well-developed crystal faces on a pale yellow, nearly gem quality, single-crystal from Fort Dauphin, Madagascar (designated as OFD) allowed identification of faces (001) and (010). The third orientation (100)* was cut perpendicular to these faces. Sample composition (Table 1) corresponds to the formula $K_{0.92}Na_{0.08}Al_{0.99}Fe^{3+}_{0.005}Si_{2.95}O_8$. No evidence of H was seen in polarized IR spectra, indicating that total water content is below a few ppm. Data along [001] were acquired from a smaller sample (Mt. Tananarive, Madagascar), which is also dry, designated as OMT. We emphasize that the (001) face was used, so the orientation is not exactly the same as (001)* of OFD. The formula for OMT is $K_{0.95}Na_{0.05}Al_{0.96}Fe^{3+}_{0.04}Si_{3.00}O_8$; OMT has more Fe and less Na substitutions than OFD. Both specimens were purchased from Excalibur Mineral Company.

This locality has historically been described as orthoclase. Recent X-ray studies on samples chemically similar to OMT with formula $(K_{0.95}Na_{0.05})[Al_{0.95}Fe^{3+}_{0.05}Si_3O_8]$ but from Itrongay are monoclinic (*C*2/*m*), highly disordered, characteristic of low-sanidine (0.352 Al in the $T_1$ site) with Fe enriched on $T_1$ (Nyfeler et al. 1998). Ackermann et al. (2004) found that Fe is fully ordered on the $T_1$ site. Our samples should be similar.

In preparing glass O from the OFD crystal, some K was lost: the formula is $K_{0.81}Na_{0.09}Al_{0.97}Fe^{3+}_{0.016}Si_{3.03}O_8$. Only a few large bubbles exist and these were avoided in laser-flash analysis. Two other glasses with near-ideal $KAlSi_3O_8$ composition were examined. From Table 1, glass S has a formula $K_{1.02}Al_{0.96}Si_{2.95}O_8$ and glass W has a formula $K_{0.98}Al_{1.04}Si_{2.92}O_8$. The principal difference between the two glasses is their thermal history. Glass S was quenched from high temperature, resulting in glass lumps that are under tension and that easily fractured during sample preparation. Glass S also has several bubbles of 0.5–1 mm in diameter. Glass W was also quenched directly from high temperature, but about half of the batch was subsequently annealed over the period of 1 day by slowly heating to ~30°C above the nominal glass transition, followed by slow cooling back to room temperature. The annealed sample is referred to as $W_a$, whereas $W_{na}$ refers to the sample that was not annealed. Glass $W_a$ did not fracture as much as glasses S or $W_{na}$ during sample preparation. Overall, glass S had more and larger bubbles than glass W.

Infrared spectra for all glasses have a broad, asymmetric band near 3,550 $cm^{-1}$ (Fig. 2) as do the high silica glasses of Okamura et al. (2003). Water content decreased upon heating, significantly for both synthetic glasses, but slightly for glass O (Table 2). Sample S was initially volatile rich, but after heating this specimen has similar water content to the two other glasses.

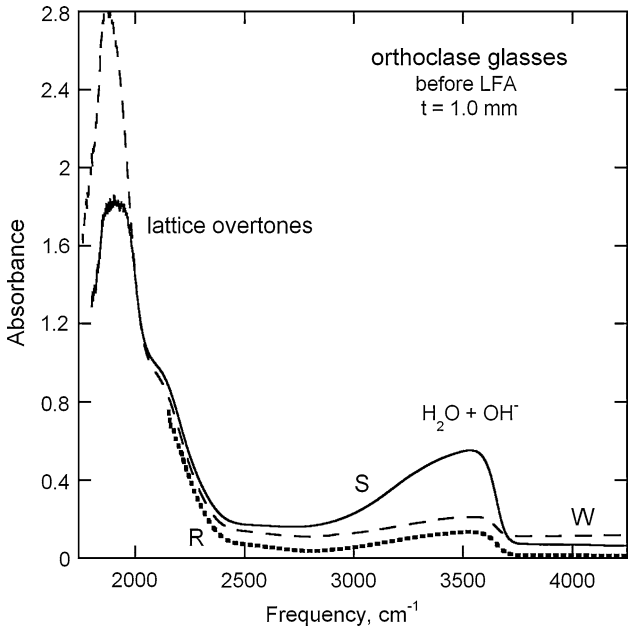


**Fig. 2** Absorption spectra from glasses prior to LFA experiments. Scaled to represent thickness of 1 mm. *Solid line* sample S, taken from $L$ = 1.747 mm, with 488 ppm as $H_2O$. *Dashed line* sample W, taken from $L$ = 1.08 mm with 101 ppm as $H_2O$. *Dots* sample R, taken from $L$ = 5.3 mm with 123 ppm as $H_2O$

**Table 2** Water content (in ppm) versus maximum temperature (in K) during LFA measurements

| Maximum run temperature | S glass | W glass | Remelt |
|---|---|---|---|
| ~298 | 434–488 | 101–122 | 123 |
| ~600 | | 84–90 | |
| ~1,100 | 98–107 | 88 | |
| ~1,300 | | 71 | 120 |
| ~1,600 | 71 | 77 | 110 |

**Table 3** Viscosity measurements on supercooled orthoclase liquids

| W glass[a] | | O glass[a] | | S glass[a,b] | |
|---|---|---|---|---|---|
| $T$ (°C) | log $\eta$ (Pa s) | $T$ (°C) | log $\eta$ (Pa s) | $T$ (°C) | log $\eta$ (Pa s) |
| 927.7 | 12.31[c] | 933.2 | 11.66 | 856.9 | 11.51[e] |
| 932.2 | 12.26[c] | 943.2 | 11.55 | 871.3 | 11.26[e] |
| 937.4 | 12.11[c] | 953.0 | 11.26 | 877.7 | 11.03[e] |
| 941.0 | 12.07[c] | 962.4 | 11.08 | 891.1 | 10.91[e] |
| 942.2 | 12.02[c] | 963.7 | 11.05 | 897.8 | 10.62[e] |
| 952.1 | 11.82[c] | 969.0 | 11.02 | 911.2 | 10.55[e] |
| 953.1 | 11.77[d] | 972.4 | 10.87 | 918.0 | 10.26[e] |
| 954.6 | 11.77[d] | 973.1 | 10.90 | 930.9 | 10.22[e] |
| 957.9 | 11.65[c] | 976.7 | 10.82 | 935.9 | 10.09[e] |
| 959.4 | 11.67[d] | 982.0 | 10.70 | 938.0 | 9.93[e] |
| 961.3 | 11.62[d] | | | 950.6 | 9.88[e] |
| 961.4 | 11.63[c] | | | 956.2 | 9.64[e] |
| 962.2 | 11.62[c] | | | 967.2 | 9.52[f] |
| 962.6 | 11.59[c] | | | 970.6 | 9.59[e] |
| 969.7 | 11.45[d] | | | 1,010 | 6.80[b] |
| 971.2 | 11.38[c] | | | 1,104 | 7.89[b] |
| 971.7 | 11.44[c] | | | 1,204 | 9.00[b] |
| 978.6 | 11.25[d] | | | | |
| 978.9 | 11.24[d] | | | 958.0 | 9.40[g] |
| 979.3 | 11.26[d] | | | 966.2 | 9.27[g] |
| 982.0 | 11.26[c] | | | 978.1 | 9.13[g] |
| | | | | 986.5 | 9.01[g] |

[a] Measured by parallel-plate viscometry at the University of Missouri, Columbia

[b] Measured by rotational viscometry at the University of California, Santa Barbara

[c,d] Superscripts indicate two separate cylinders for W glass, run 11 days apart

[e,f,g] Superscripts indicate three separate cylinders for S glass. Cylinder g has a lower viscosity than cylinders e and f, and is not used in fitting TVF equations. See text for discussion

## Results

### Viscosity

Viscosity data for two cylinders of synthetic W glass, and one cylinder of glass O (melted OFD crystal), are in Table 3 and Fig. 3. Near the glass transition, viscosity is close to a linear function of inverse temperature for both samples. Viscosity of the synthetic glass decreases by one order of magnitude, from $10^{12.3}$ Pa s at 928°C to $10^{11.3}$ Pa s at 982°C. The viscosity of O is 0.5 log units lower than that of W over the same temperature range, but the slopes and apparent activation energies are identical. The offset may be due to slight compositional differences because glass O was prepared from a natural crystal and therefore contains minor sodium and iron. The interpolated glass transition temperatures, taken to be the temperature of the $10^{12}$ Pa s. isokom ($T_{12}$), are 1,216 K for W glass, and 1,191 K for O glass, respectively.

Two cylinders of S glass yielded viscosity results that were consistent with the three higher-temperature measurements obtained using rotational viscometry, and together indicate a glass transition temperature ($T_{12}$) of 1,100 K. Measurements on the third cylinder were consistently 0.3 log units lower than for the other two.

Glass S having lower viscosity is ascribed to composition. It is slightly peralkaline (molar K/Al = 1.07), and contains ~400–500 ppm water, significantly higher than either W or O glasses (~100–120 ppm). Even trace quantities of water noticeably affect the viscosity and glass transition temperature of highly polymerized liquids such as feldspars and granites (Jewell et al. 1993). The lower viscosity of the third core suggests compositional heterogeneity within the glass

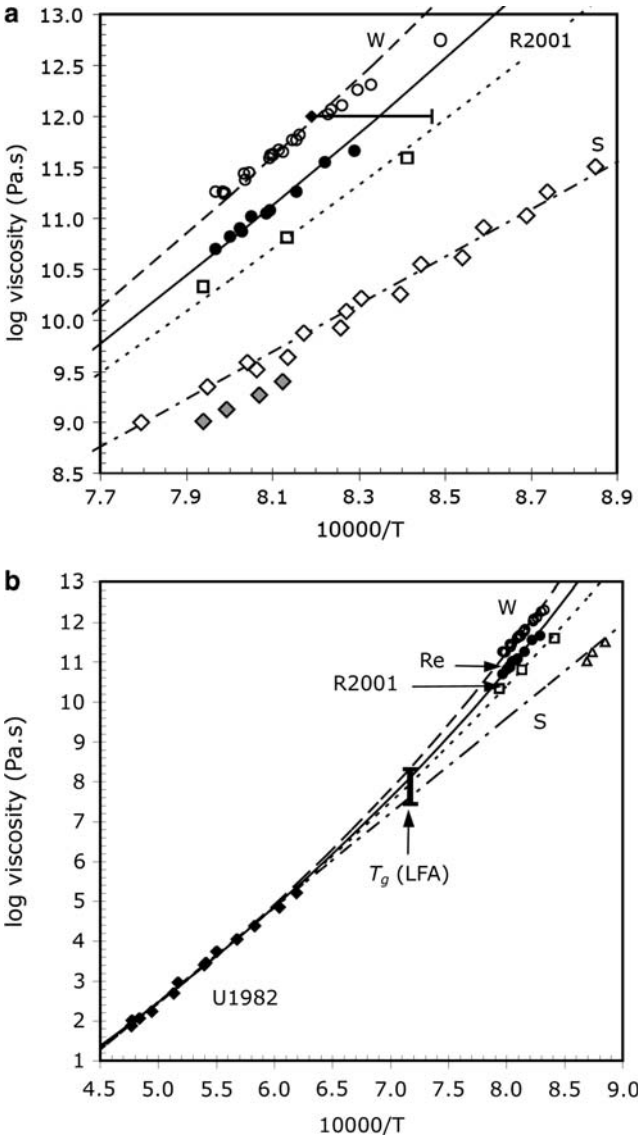


**Fig. 3** **a** Viscosity data for supercooled $KAlSi_3O_8$ liquids near the glass transition. *Open circles* W glass, *filled circles* remelted OFD glass "O", *open squares* data of Romano et al. (2001), *open diamonds* S glass, *gray diamond* S glass cylinder "g". *Filled diamond* glass transition temperature based on calorimetry measurements of Richet and Bottinga (1984); *horizontal line* indicates range of previous estimates of the glass transition (see Richet and Bottinga 1984, for discussion). Lines are TVF curves, fitted to low temperature data for individual samples combined with high temperature data from Urbain et al. (1982). See text and Table 5 for details. **b** Viscosity data for $KAlSi_3O_8$ liquids. *Filled diamonds* high-temperature data of Urbain et al. (1982), *bracket* at 1,400 K indicates glass transition observed in LFA measurements of *D*. Other symbols as for **a**

sample, either in major element composition or water content. Similar differences were measured between two cores taken from a commercially prepared $NaAlSi_3O_8$ glass by Whittington et al. (2004), and serve to underscore the importance of careful sample characterization when interpreting data for highly polymerized aluminosilicate glasses.

The viscosity difference between cores from the same glass is small compared to the difference between S glass and the other samples studied (Fig. 3).

## Thermal diffusivity of low-sanidine single crystals

At room temperature, thermal diffusivity values for the two principal crystallographic orientations, faces (001), (010) and the orthogonal face (100)* of OFD are 1.11, 1.34 and 0.80 $mm^2\ s^{-1}$, respectively. One additional measurement from planes of the type (x0z) is needed to define the principle axes in *x*–*z* planes (Nye 1985). Due to the similar values of *D* for heat propagating along [001] and [100]*, the similar values form OFD along [100]* and OMT along [100], the unpolarized nature of our measurements, the manner in which heat (light) propagates in *C*2/*m* crystals (e.g., Zulumyan et al. 1976), and because heat transfer in *C*2/*m* pyroxenes is tied to the crystallographic axes (Hofmeister and Pertermann, in review), we did not characterize a fourth direction for OFD. Specifically, OMT [100] being larger than OFD [100]* is consistent with the orthogonal orientations [100]* and [001] of OFM defining the maximum and minimum directions of *D* in the *x*–*z* plane, presuming that slight differences in chemical composition do not affect the temperature values (Fig. 4, Table 4). In addition, only two types of IR modes exist: the $A_u$ species,

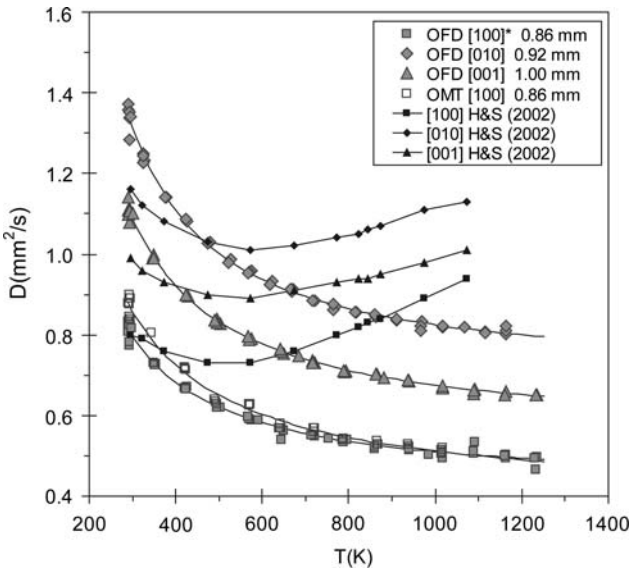


**Fig. 4** Thermal diffusivity of orthoclase single-crystals as a function of temperature. *Open or grey symbols* LFA, this study. *Filled symbols* single-contact method, Höfer and Schilling (2002). *Solid lines* interpolations between data points. *Gray symbols* OFD faces: *square* (010); *triangle* (001); *diamond* (100)*. For ONT (*open*) and the previously study (*black*), the same symbols were used, except that the orientation is along [100], not [100]*. *Broken curves* least-squares fits of Table 2

**Table 4** Thermal diffusivity values and fitting parameters

| Sample | Thickness (mm) | $T$ (°C) | $D$ (mm$^2$/s) | $n$ | $T$ (°C) | $D$ (mm$^2$/s) | $n$ | Fitting parameters | | | | Notes |
|---|---|---|---|---|---|---|---|---|---|---|---|---|
| | | | | | | | | $a$ | $b$ | $c$ | $R^2$ | |
| Single crystal | | | | | | | | | | | | |
| OFD [100]* | 0.86 | 19 (1) | 0.80 (2) | 7 | 890 (1) | 0.50 (1) | 3 | 0.4183 | 82.33 | 9,356.8 | 0.992 | |
| OFD [010] | 0.92 | 19 (1) | 1.34 (3) | 5 | 890 (1) | 0.81 (1) | 3 | 0.6990 | 99.88 | 25,726.6 | 0.996 | |
| OFD [001] | 1.00 | 20 (1) | 1.11 (2) | 7 | 890 (1) | 0.66 (1) | 3 | 0.5492 | 110.40 | 15,574.4 | 0.998 | |
| OMT [100] | 0.86 | 20 (1) | 0.87 (2) | 6 | 743 (1) | 0.51 (1) | 3 | 0.3896 | 114.07 | 8,136.1 | 0.99 | |
| Glasses | | | | | | | | | | | | |
| Wna | 1.08 | 19 (1) | 0.59 (1) | 20 | 595 (3) | 0.53 (1) | 3 | 0.5154 | 3.803 | 5,482.0 | 0.937 | Heated to 600°C |
| Wna | 1.08 | 20 (1) | 0.60 (1) | 7 | 987 (1) | 0.56 (1) | 3 | 0.5668 | 38.431 | 14,261.8 | 0.901 | First heating > $T_g$ |
| Wna | 0.86 | 20 (1) | 0.62 (1) | 8 | 988 (1) | 0.54 (1) | 3 | 0.5401 | −2.653 | 7,599.0 | 0.964 | Second heating > $T_g$ |
| Wna | 0.82 | 17 (1) | 0.61 (1) | 3 | 992 (2) | 0.52 (1) | 2 | | | | | First heating > $T_g$ |
| Wna | | | | | 1,279 (1) | 0.48 (1) | 1 | | | | | Melt proxy |
| Wna | 0.775 | 19(1) | 0.60 (1) | 11 | | | | | | | | Post 1,300°C |
| Wa | 0.81 | 20 (1) | 0.62 (1) | 6 | 994 (1) | 0.54 (1) | 3 | 0.5304 | −0.4577 | 7,482.5 | 0.977 | First heating > $T_g$ |
| Wa | 0.77 | 21 (1) | 0.62 (1) | 4 | 986 (1) | 0.53 (1) | 2 | 0.5132 | 17.152 | 4,214.4 | 0.986 | Second heating > $T_g$ |
| S | 0.74 | 20 (1) | 0.60 (1) | 8 | 984 (1) | 0.50 (1) | 3 | 0.4848 | 19.89 | 4,071.9 | 0.983 | Second heating > $T_g$ |
| S | 0.71 | 19 (1) | 0.59 (1) | 3 | 1,260 | 0.484 (5) | 2 | | | | | Third heating, melt proxy |
| S | 0.71 | | | | 1,350 (1) | 0.476 (5) | 3 | | | | | Melt proxy |
| O1 | 1.018 | 20.7 | 0.58 (1) | 8 | | | | | | | | First heating > $T_g$ |
| O2 | 0.705 | 19 (1) | 0.59 (1) | 4 | 1,062 (1) | 0.506 (1) | 3 | | | | | First heating > $T_g$ |
| O2 | 0.705 | | | | 1,375 (1) | 0.466 (3) | 3 | | | | | Melt proxy |
| O2 | 0.68 | | | | 1,299 (1) | 0.48 (1) | 2 | | | | | Melt proxy |
| O2 | 0.60 | 21 (1) | 0.61 (1) | 7 | 923 (2) | 0.52 (1) | 3 | 0.52615 | −9.1562 | 9,920.3 | 0.993 | Post 1,400°C |

and the $B_u$ species. The $A_u$ species is excited when light is polarized along the $y$ axis (the orientation [010], whereas the $B_u$ species is stimulated when the electric vector lies somewhere in the $x$–$z$ plane, such that $B_u$ vibrations do not necessarily orient with the crystallographic axes or the optical axes. Because our measurements are unpolarized, for (010) slabs all the $B_u$ modes are excited, if we view heat as phonons moving perpendicular to the slab faces. The $B_u$ modes are stimulated because the electric vector of the phonons is perpendicular to the direction of propagation. For the other slabs, all the $A_u$ species and some of the $B_u$ modes are involved in heat transport.

With increasing temperature, thermal diffusivity of the crystal decreases and approaches a constant value at high temperature (Fig. 4). At 1,163 K, $D_{[100]*}$, $D_{[010]}$ and $D_{[001]}$ are 0.50, 0.81 and 0.66 mm$^2$ s$^{-1}$, respectively. Runs were terminated at 1,270 K to avoid possible pre-melting effects. Table 4 provides parameters for the fit:

$$D = A + B/T + C/T^2. \quad (4)$$

This form reasonably reproduces diffusivity data over the entire measured temperature range for the single crystals and the glasses at temperatures below the glass transition, where $D$ drops abruptly. Alternative fits such as

$$1/D = a + bT + cT^2 \quad (5)$$

do not reproduce data well at $T$ above 600 K for the glass.

## Thermal diffusivity of potassium feldspar glasses

We found that samples must be very thin for results to be reproducible, and for such thin samples (~0.7 mm), parallelism of the surfaces is important. Specifically, increasing $D$-values were seen from ~1,100 K to $T_g$ for thick samples (>1 mm for 15 mm diameter, $d$), but not thin samples (≤0.8 mm, Fig. 5). More extreme upturns were seen for glass O with thickness $L$ = 1.0 mm for 9-mm diameter (not shown), which decreased upon thinning to 0.8 mm, but were still present. The upturn did not exist for a second chip of the same batch with $L$ = 0.8 mm and diameter of 10 mm (Fig. 6). The cause of the upturns could be an excessive temperature difference across the sample (>10 K), which violates model assumptions, or edge effects. For olivines with $D$ ~ 2 mm$^2$ s$^{-1}$, we found that ratios of $L/d$ ~ 1/10 are needed (Pertermann and Hofmeister 2006), but for glasses with very low thermal diffusivity, even thinner samples are required. The

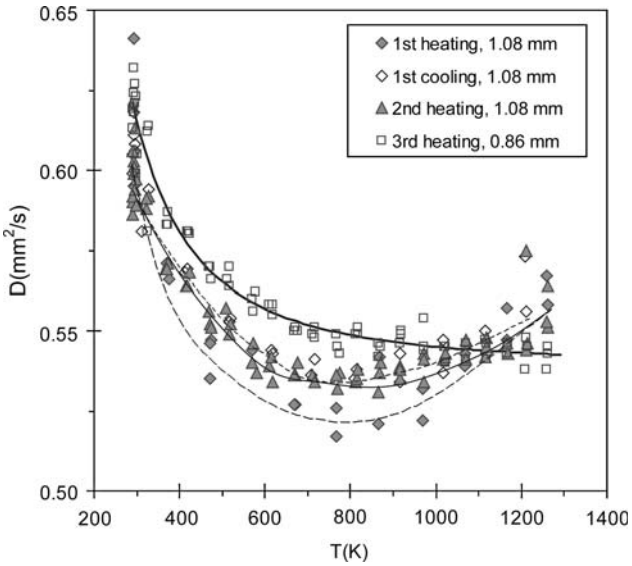


**Fig. 5** Thermal diffusivity of orthoclase glass W, showing effects of annealing, thermal history, and thickness. *Symbols* are described in the box: corresponding values are in Table 3. Note the highly expanded *Y*-axis. Overly large thickness causes the upturn in *D* above 1,000 K

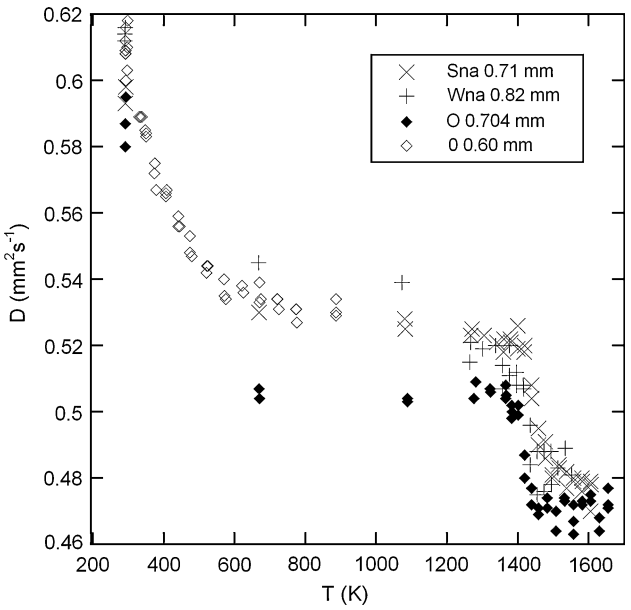


**Fig. 6** Thermal diffusivity of three glasses. *Symbols* as labeled

remainder of the report concerns thin ($L/d < 1/12$) samples.

To probe the effect of thermal history, one glass sample (*W*) was repeatedly heated in LFA experiments, as well as being annealed prior to measurements. This sample was used because it dehydrates very little during our experiments (Table 2) and is nearly homogeneous in water content. Figure 7 shows that *D* is higher for the annealed sample and *D* increases after repeated heating in the LFA apparatus, attributed to removal of residual strain in the

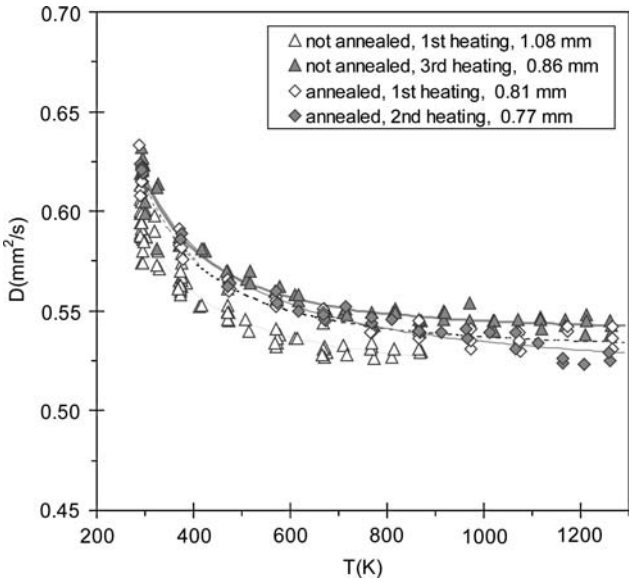


**Fig. 7** Effect of annealing on thermal diffusivity for glass W. *Symbols* as labeled

particular sample through repeated heating episodes. However, the differences are small and close to the experimental uncertainties of $\sim$0.01 mm$^2$ s$^{-1}$: thermal diffusivity at 298 K for partially annealed glass samples, regardless of slight differences in chemical composition, are 0.58–0.62 mm$^2$ s$^{-1}$.

High-temperature values also depend weakly on composition or thermal history. For all three glasses, *D* decreases with *T* up to $\sim$800 K. From $\sim$800 K up to the temperature ($T_g$) of 1,370 K, a constant value $D_{sat}$ of 0.50–0.56 mm$^2$ s$^{-1}$ is observed, with the higher value being associated with sample W (Figs. 5, 6 and 7). Based on viscosity measurements of the liquid (Fig. 3), $\sim$1,370 K in diffusivity measurements corresponds to a viscosity of about $10^{8.2}$ to $10^{7.2}$ Pa s, and a relaxation time-scale of $\sim$1 to 10 ms, consistent with the duration of the laser pulse ($\sim$1 ms), and is thus the glass transition temperature in our heat transfer experiments.

From $T_g$ to about 100° higher, *D* decreases rapidly and then levels off to another constant value ($D_{melt}$ = 0.466 to 0.484 mm$^2$ s$^{-1}$, Table 4) that is maintained to the highest temperatures accessed (1,650 K). Although this state is supercooled (metastable) melt, we use this subscript to emphasize that the thermal diffusivity above $T_g$ should represent that of the melt up to and including superliquidus conditions. First, for silicates and oxides (both glasses and crystals) studied so far, constant *D* is observed at some high temperature. This behavior is termed saturation, as the effect is attributable to phonon populations ceasing to increase with temperature (Hofmeister 2006, 2007b; Pertermann and Hofmeister 2006; Hofmeister et al. 2006; Hofmeister and Yuen 2007; Branlund and Hofmeister 2007). Here, nearly

constant $D$ was observed for the orthoclase crystal above ~1,000 K, near several hundred degrees below $T_g$ for all three glasses, and above $T_g$ for supercooled liquid. Because feldspathic liquids have small configurational heat capacities (Richet and Bottinga 1984), further changes in $D$ due to structural changes are expected to be very minor between $T_g$ and superliquidus temperatures.

Dehydration to roughly similar values after high-$T$ experiments (Table 2) and annealing to similar temperatures to remove thermal history effects, allows isolation of the effect of variations in cations other than H. Glass O, prepared from natural crystal OFD, has substantial Na, whereas sample S is slightly high in K and low in Al, and sample W is slightly low in K and Si. For similarly dry and partially annealed glasses, both room temperature values and $D_{sat}$ follow the order W ≥ S ≥ O (Tables 2, 4; Fig. 6). However, $D_{melt}$ is similar for all three samples. We conclude that the slight departures from orthoclase stoichiometry, regardless of the type of substitution, have little to no effect on thermal diffusivity of the liquid.

Sample S was dehydrated significantly during repeated heatings (Table 2). The data are not sufficient to isolate the effect of H content, because thermal history is intertwined with dehydration (Table 4) and because about 1,000-ppm water is needed for the difference in $D$ due to OH to be substantially larger than the uncertainty in the measurement (Hofmeister et al. 2006).

### Comparison of $D$ for crystal, glass, and melt

Compared to the crystals, $D$ of the glasses has a weaker temperature dependence (Fig. 8). Near 800 K, $D$ for the glass is roughly equal to that of the most insulating orientation, [100], and $D$ of the glass is slightly larger than [100] near $T_g$, but at all temperatures, $D$ of the bulk crystal (the average of the three orientations) is greater than that of the glass. About 100 K above the glass transition, $D$ of the glass drops below that of [100] single crystals. We conclude that $D$ of the melt is ~25% lower than that of the analogous crystal projected forward in temperature.

## Discussion

### Comparison to previous results on viscosity

Previous studies of $KAlSi_3O_8$ near the glass transition are few. Three viscosity data were published by Romano et al. (2001), and plot 0.4 log units lower than for molten O, 0.9 log units lower than for molten W, and ~1.0 log units higher than molten S (Fig. 3). From Romano et al. (2001), $T_{12}$ is 1,167 K, compared to 1,216 K for $W$, although both samples are synthetic and slightly peraluminous. Remelted

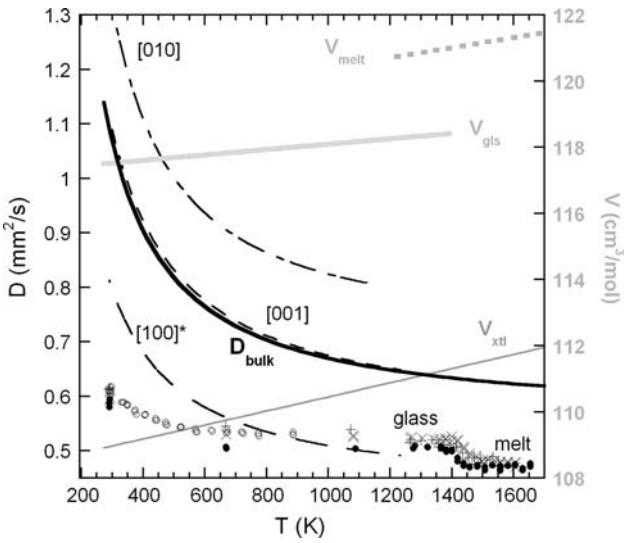


**Fig. 8** Comparison of thermal diffusivity for crystals, glass, and melt. *Gray* volume data, see text for sources. *Dots* melt; *thick line* glass; *thin line* bulk crystal. *Black* fits to $D(T)$. *Dash-dots* (010); *short dashes* (001); *long dashes* (100)*. The three glass samples, including the "melt" region are shown as *circles* (2 runs for sample, *open circle*), *plus symbol* for sample Wna and × for sample Sna

natural orthoclase lies between the two. Richet and Bottinga (1984) suggested that the glass transition temperature of $KAlSi_3O_8$ is 1,221 K, based on their drop calorimetry data, although previous estimates summarized in that paper range from 1,180 to 1,220 K. The glass transition temperature and viscosity of molten $NaAlSi_3O_8$ is known to be very sensitive to composition (Richet and Bottinga 1984), with the viscosity of $Na_2O$–$Al_2O_3$–$SiO_2$ liquids reaching a maximum at peraluminous compositions (Toplis et al. 1997), and it is likely that the viscosity–composition relations of $KAlSi_3O_8$ liquids are similar.

High-temperature viscosity data for $KAlSi_3O_8$ collected at 1-atm pressure by Urbain et al. (1982) are combined with the low temperature data presented here to interpolate the viscosity of the samples at intermediate temperatures (Fig. 3b). The combined datasets were fitted with the Tamman–Vogel–Fulcher (TVF) equation:

$$\log \eta = A + B/(T - C), \quad (6)$$

where $A$, $B$ and $C$ are adjustable parameters. The best-fit values of $A$, $B$ and $C$ for the high-temperature data of Urbain et al. (1982) combined with the low-temperature data for W glass, S glass, remelted O glass, and Romano et al. (2001) are given in Table 5. Despite the variation in the viscosity data at the glass transition, all three TVF equations indicate near-Arrhenian behavior, characteristic of a "strong" liquid, and result in a small range of interpolated viscosity at 1,470 K, the highest temperature reached during thermal diffusivity measurements.

**Table 5** Fits to viscosity data of the form: $\log \eta = A + B/(T - C)$ where $T$ is in Kelvin and $\eta$ is in Pa s

| T (°C) | $A$ | $B$ | $C$ | $T_{12}$ (°C) | $n$[a] | rms error[b] |
|---|---|---|---|---|---|---|
| W glass | −5.98 | 12,371 | 530.7 | 945.6 | 34 | 0.09 |
| OFD remelt | −6.03 | 12,883 | 483.3 | 924.7 | 23 | 0.07 |
| Romano[c] | −6.80 | 15,062 | 373.7 | 901.7 | 16 | 0.08 |
| S glass[d] | −9.15 | 23,266 | 0.0 | 826.9 | 31 | 0.13 |

[a] $n$ = number of data used in the fit. Total number includes 13 data points from Urbain et al. (1982)

[b] rms error is calculated based on fit to data for the sample and the data of Urbain et al. (1982)

[c] Three data points for $KAlSi_3O_8$ from Romano et al. (2001)

[d] The zero value for $C$ makes this an Arrhenian equation; the best fit returns a negative value for C (within uncertainty of zero), which is unphysical

## Comparison to previous results on $D$: inference of problems in contact methods

Höfer and Schilling (2002) also examined Madagascar low-sanidine, using a single contact method wherein heating is from a remote source but a thermocouple is attached to the sample for measurement of the time-temperature response, which we refer to as RHTM. From X-ray fluorescence measurements, their sample has more Fe (1.21 wt% $Fe_2O_3$) substituting for Al, and less Na (0.62 wt% $Na_2O$), and thus the degree of solid solution is about the same, although the specific atoms being substituted differ. Such slight differences in chemical composition are unlikely to be important, given our results for $D$ from two different crystals and the three different $KAlSi_3O_8$ glasses, and previous measurements of olivines and garnets (Pertermann and Hofmeister 2006; Hofmeister 2006). The significant differences between the present results and those of Höfer and Schilling (Fig. 4) are therefore due to experimental technique. The increase in $D$ with $T$ above ~600 K in RHTM experiments is due to direct radiative transfer, as discussed by Höfer and Schilling (2002). These authors consider radiative transfer to occur above ~800 K, but from Fig. 4 and our own time–temperature curves (Fig. 1), it is seen that direct radiative transfer occurs at all temperatures. The temperature dependence of $D$ seen in the RHTM data is not intrinsic to their samples, and does not portray lattice thermal diffusivity of transparent feldspar.

Milky orthoclase from Japan was also studied using RHTM. The resulting $D$ values (not shown) are nearly independent of temperature (Höfer and Schilling 2002). Given that dunite, which has substantial physical scattering, and gem-quality olivine of similar compositions have the same decrease in $D$ with $T$ (Pertermann and Hofmeister 2006), we conclude that the RHTM data at temperature on milky orthoclase is only slightly impacted by spurious direct radiative transfer.

Near 298 K, $D$ from RHTM is lower than that from LFA by 12% for [010], 10% for [001] using sample OFD, and 10% for [100] using sample OMT (Fig. 4). The consistency of the comparison indicates that the differences between $D$ along [100]* of OFD and along [100] of OMT are orientational, and supports our contention that the minimum and maximum directions were defined by the three orthogonal orientations of OFD. Because direct radiative transfer increases apparent values of $D$, reduced values are ascribed to thermal resistance at the interfaces. Imperfect contact creates gaps through which phonons cannot propagate (e.g. Freid 1969). For olivine and quartz, RHTM gives similar offsets of 12 and 5%, respectively, averaged over the various orientations (Hofmeister 2007a, b).

Other measurements of feldspars are available (e.g., Sass 1965), but some studies are limited to room temperature and others do not include chemical compositions. All such early data are made using contact methods, which will have problems similar to those of the RHTM method discussed above and hence, comparison with data in the geologic literature is not made. Cryogenic measurements of $k$ for feldspars exist (Cahill et al. 1992), and are discussed below.

A few direct measurements of thermal diffusivity of melts have been made using contact techniques. Although the compositions differ from ours, some discussion is in order, given the problems associated with conventional methods. Snyder et al. (1994) examined diopside melt. Their approach attempts to correct for radiative transfer. Unfortunately, the formulae used are appropriate for diffusive radiative transfer, which does not occur in experiments as the length scales are short compared to length scales over which light is attenuated, especially at frequencies where the material is transparent (the near-IR), see Pertermann and Hofmeister 2006 and Hofmeister et al. (2007) for further discussion. Due to the strong dependence of the inapplicable formulae on temperature ($T^3$), the inferred temperature dependence of thermal conductivity of diopside melt is likely to be incorrect. As their lowest temperature is the least impacted, comparison is made with this value (0.31 W $m^{-1}$ $K^{-1}$), which translates to $D$ = 0.07 $mm^2$ $s^{-1}$ using $\rho \sim 2.69$ g $cm^{-3}$ and $C_P \sim$ 340 J $mol^{-1}$ $K^{-1}$ (from data compiled by Stebbins et al. 1984). This value of $D$ for diopside melt is one-seventh of our results for orthoclase melt. Bagdassarov and Dingwell (1994) applied another contact method to rhyolite. Adjustments for radiative transfer (shown as an upturn in $D$ at ~800 K) similarly involved an inapplicable $T^3$ relationship. For rhyolite (actually glass) at 298 K, their $D$ is ~0.08 $mm^2$ $s^{-1}$, which is ~1/7th of our present result of ~0.6 $mm^2$ $s^{-1}$ for orthoclase glass, and 1/11th that of silica glass ($D \sim 0.9$ $mm^2$ $s^{-1}$, Hofmeister et al. 2006).

Although the compositions differ, we suggest that the previous measurements of glass and melt are low, due to

the approximations made to correct for radiative transfer and possible interface resistance. LFA experiments on a wider range of compositions would be worthwhile.

## Thermal conductivity of $KAlSi_3O_8$ crystal, glass, and liquid calculated from trends in $D$

Equation 1 was used to compute $k$, using the fits for $D(T)$ in Table 4. For $C_P$ of melt, we used the temperature-independent value of 367 ± 4 J mol$^{-1}$ K$^{-1}$ (Lange 2007 based on Stebbins et al. 1983 and Richet and Bottinga's 1984 results]. For glass,

$$C_p(T) = 511.51 - 5076.7\,T^{-0.5} + 205410\,T^{-2} - 0.034885\,T \quad (7)$$

(Richet 1987). For crystal, we used the fit for sanidine suggested by Lange (2007):

$$C_p(T) = 382.37 - 1941.0\,T^{-0.5} - 12037300\,T^{-2} + 1836430000\,T^{-3}. \quad (8)$$

For density, we used inverse volume in cm$^3$ mol$^{-1}$ for an 8-oxygen formula. Lange's (2007) model was used for the melt:

$$V(T) = 118.893 + 0.00151\,T \quad (9)$$

Our data on glass volumes are described by

$$V(T) = 117.28 + 0.00081426\,T. \quad (10)$$

Thermal expansivity is lower for the glass in part because the liquid has a configurational component. At room temperature, Hovis et al. (1999) determined sanidine volume as 108.996 cm$^3$ mol$^{-1}$ and volumetric thermal expansivity as 19.3 × 10$^{-6}$ K$^{-1}$. Data on the axes are unavailable. We therefore approximated $k$ for the orientations, from the unit cell volume.

From Fig. 9, it is seen that thermal conductivity of the bulk crystal and the three orientations is nearly constant, but decreases almost linearly with temperature. Bulk $k$ (in W m$^{-1}$ K$^{-1}$) is described by

$$k_{bulk}(T) = 2.073 - 0.00025819\,T + 7.0057 \times 10^{-8}\,T^2 \quad (11)$$

where $R$ = 0.9985. For the glass, $R$ = 0.9989 for

$$k_{gls}(T) = 0.67358 - 0.0019023\,T - 1.6203 \times 10^{-6}\,T^2. \quad (12)$$

For the melt, R is near unity for

$$k_{mlt}(T) = 1.4657 - 1.79510057 \times 10^{-5}\,T. \quad (13)$$

Given the uncertainties, $k$ of glass and melt are equal and nearly constant (1.45 W m$^{-1}$ K$^{-1}$) above 1,200 K. The asymptotic value for the bulk crystal is 1.83 W m$^{-1}$ K$^{-1}$.

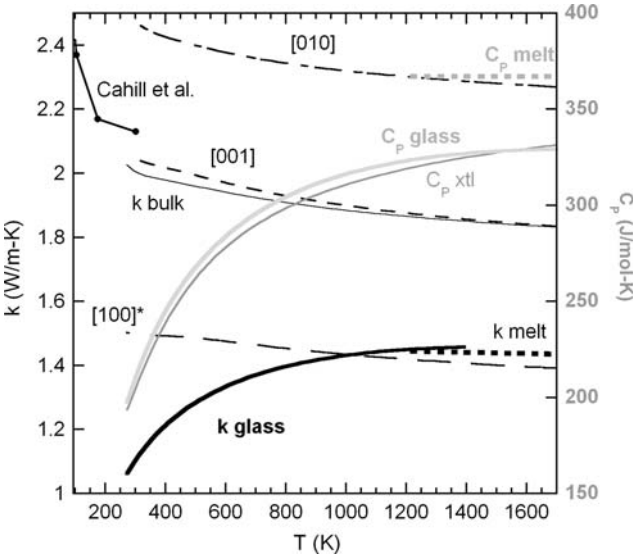


**Fig. 9** Comparison of thermal conductivity of crystal, glass and melt. *Gray* heat capacity data, see text for values. *Black* thermal conductivity calculated as described in the text. Orientations and species are as labeled. *Dots* contact measurements of Cahill et al. (1992) which mix polarizations. *Other symbols* as in Fig. 8

Cahill et al. (1992) measured $k$ from a sample of Madagascar potassium feldspar using the 3-$\omega$ method. The orientation was not specified. This method is free of radiative transfer effects, but use of a radial geometry mixes the two polarizations. It is a single-contact method, so some contact resistance may exist. Values are in reasonably good agreement with (001) near room temperature, and just below 298 K, the slope is flat, as in our results (Fig. 9). Their results are larger than our bulk values, probably because their orientation contains a substantial contribution from (010).

## Comparison with theory

The observed behavior with temperature is consistent with the damped harmonic oscillator model of the phonon gas:

$$D(T) = \frac{\langle u(T)\rangle^2}{6\pi Z\langle \mathrm{FWHM}(T)\rangle} = \frac{\langle u(T)\rangle^2\langle \tau(T)\rangle}{3Z}. \quad (14)$$

where $\langle u\rangle$ is an average sound speed, $Z$ is the number of formula units in the primitive cell, and $\langle$FWHM$\rangle$ is the average full width at half maximum of the peaks in the dielectric function (Hofmeister 2006). Mean free lifetimes $\langle\tau\rangle$ of the phonons decrease smoothly with $T$, largely due to increasing the number of states populated. This number increases because higher $T$ activates higher frequency modes. However, no modes are observed at very high frequency (>∼2,500 cm$^{-1}$) because discrete states do not exist: due to large, finite bandwidths, the overtone-combination

modes provide a continuum (Mitra 1969). Therefore, $D$ decreases with $T$, but once a certain high temperature is reached, lifetimes, FWHM and $D$ all become constant. The saturation temperature is low for orthoclase glasses because its bands are broad and the continuum is reached at lower temperature.

The dependence of $D$ on structure is also consistent. Melt is more disordered than glass, which is more disordered than crystal. FWHM decreases in this same order, causing $D$ to increase in this order, at a given temperature. Sound speeds have an effect, but the variation is not large, so that FWHM dominates. This finding suggests that isochemical melting of any material should produce lower $D$-values. In particular, we expect this to be the case for silicic rocks, based on results for orthoclase here and commercial glass data elsewhere (Hofmeister et al. 2006). Note that potassium feldspars from Madagascar are highly disordered (e.g., Nyfeler et al. 1998), and thus lower-temperature species that are more highly ordered will have even higher $D$ and $k_{lat}$ relative to glasses and melts.

The increase in $k$ with $T$ for glass seen here has previously been observed for other compositions via contact methods, and has been designated as "glass-like behavior" (e.g., Cahill et al. 1992). This behavior contrasts with the observations of crystals, wherein $k$ decreases as $T$ increases. This is not a radiative transfer effect in our measurements. The increase in $k$ with $T$ results from the convolution of the temperature dependences of $D$, $C_P$, and $\rho$ to provide $k$ (Eq. 1). Density decreases almost linearly and weakly with temperature for most materials. For glasses, $D$ decreases weakly as $T$ increases, whereas for crystals, the decrease is much stronger. The strong increase of $C_P$ with $T$ overcomes the weak dependence of $D$ on $T$ for glasses causing $k$ to increase with $T$. Therefore, diffusion of heat via vibrations in melts, glasses, or crystals does not differ in any fundamental manner. The temperature response of thermal conductivity is more complicated because of the contrasting behavior of $D$ and $C_P$ at low $T$, but at high $T$, saturation exists in both, providing the nearly constant trends. Thermal diffusivity is simple and easier to understand and describe than thermal conductivity. The focus on thermal conductivity is historical, and stems from the connection of flux with temperature gradients (Fourier's law) and its practical application to geotherms, as well as from the experimental developments, $k$ being easier to measure and therefore the focus of the oldest studies.

Microscopic behavior of the solid is easiest to understand (and represent) in the form $1/D$, which is closely tied to $C_V$, and thus to the measured heat capacity $C_P$ which differs from $C_V$ generally by $\sim$1–3%. Parallelism exists between $1/D$ and $C_V$ because both depend directly on the population of vibrational states. Saturation of $1/D$ (which cannot be distinguished from that of $D$) is analogous to the Dulong–Petit limit of $C_V$. The behavior of $1/D$ with all temperature is fairly simple as discussed in examining garnets and spinels, for which $D$ and/or $k$ are available over extreme $T$ ranges (Hofmeister 2006, 2007b). Magnetic and displacive phase transitions provide a $\lambda$ curve in $1/D$ as in measurements of $C_P$ (Branlund and Hofmeister 2007; Hofmeister 2007b). For the present case , both $1/D$ and $C_P$ increase by steps for the transitions from crystal to melt or glass to melt.

## Conclusions and implications

Contact-free, laser-flash analysis provides data on the lattice component of heat transfer only: systematic errors due to interface resistance and spurious radiative transfer are avoided. These attributes and the high accuracy of the technique allow resolution of the glass transition in data on $D$ of $KAlSi_3O_8$, and show that $D$ of the melt is slightly lower than that of the orthoclase glass which in turn is slightly lower than that of the average orthoclase crystal. At high temperatures, $D$ is constant, consistent with phonon saturation and the damped harmonic oscillator model. The decrease in $D$ from (crystal > glass > melt) is attributed to disordering.

Our results show that $D$ of the melt is 25% lower than that of the bulk crystal (and slightly lower than any orientation) for orthoclase. Similar behavior was seen for a commercial glass with elements B–K–Al–Na–B–Si–O, such that $SiO_2$ at 79.6 wt% is the dominant component (Hofmeister et al. 2006). We suggest that the behavior observed here for $D$ is expected for all high-silica compositions, and thus describes continental material in general. Thermal conductivity of the melt is expected be lower than the analogous crystal for other silica-rich compositions, given the behavior of density (or volume) and heat capacity for other systems (see review by Stebbins et al. 1984). Therefore, once partial melting commences in a mantle or crustal volume, heat transport by conduction is impeded. This represents a positive feedback effect. Time-dependent thermal modeling in which the effects of heat transport by advection associated with differential movement between melt and solids is included along with phonon conduction is needed to evaluate the importance of possible feedback between the rate of melt generation and decreasing phonon conduction in the melt.

Our results for orthoclase crystals should represent other feldspars as this mineral family tends to be disordered either by cation substitution or Al/Si exchange or both. The results suggest that continental crust is a much poorer conductor of heat than oceanic crust ($k$ of orthoclase is one-third that of olivine with $k = 6$ W m$^{-1}$ K$^{-1}$; Pertermann and Hofmeister 2006, using tabulations of $C_P$ and $\rho$ by

Anderson and Isaak 1995). Placement of the insulating continents over mantle downwellings, and more conductive mafic rocks over mantle upwelling leads to efficient expulsion of heat from the Earth overall. Diffusive radiative transport is not expected for much of the continental crust, due to relatively low temperatures, although this matter warrants confirmation through optical spectroscopic measurements and calculations. Overall, our results indicate the importance of further experimental studies of phonon conduction in geomaterials especially in glass, metastable (supercooled) liquids and equilibrium liquids. There have been relatively few measurements of thermal diffusivity and thermal conductivity in such materials and many of the existing measurements are compromised by simultaneously entangled contact and radiative effects.

**Acknowledgments** MP and AMH were supported by National Science Foundation (NSF) grant EAR-0207198. AGW was supported by NSF grant EAR-0440119. FJS acknowledges support from the NSF grants EAR-0609680 and EAR-0440010 as well as support from the US Department of Energy DE-FG03-91ER-14211.

## References

Ackermann S, Hänni H, Kunz M, Armbruster T, Schefer J (2004) Cation distribution in a Fe-bearing K-feldspar from Itrongay, Madagascar: a combined neutron- and X-ray single-crystal diffraction study. Schweiz Mineral Petrograph Mitt 84:345–354

Anderson OL, Isaak DG (1995) Elastic constants of mantle minerals at high temperature. In: Ahrens TJ (ed) Handbook of physical constants. American Geophysical Union, Washington DC, pp 69–96

Bagdassarov N, Dingwell D (1994) Thermal properties of vesicular rhyolite. J Volcan Geotherm Res 60:179–191

Blumm J, Lemarchand S (2002) Influence of test conditions on the accuracy of laser flash measurements. High Temp High Pres 34:523–528

Blumm J, Opfermann J (2002) Improvement of the mathematical modeling of flash measurements. High Temp High Pres 34:515–521

Branlund JM, Hofmeister AM (2007) Thermal diffusivity of quartz to 1000°C: effects of impurities and the $\alpha$-$\beta$ phase transition. Phys Chem Miner 34:581–595

Cahill D, Watson SK, Pohl RO (1992) Lower limit of thermal conductivity of disordered solids. Phys Rev B 46:6131–6140

Degiovanni A, Andre S, Maillet D (1994) Phonic conductivity measurement of a semi-transparent material. In: Tong TW (ed) Thermal conductivity, vol 22. Technomic, Lancaster, pp 623–633

Fried E (1969) Thermal conduction contribution to heat transfer at contacts. In: Tye RP (ed) Thermal conductivity, vol 2. Academic, London, pp 253–275

Getson JM, Whittington AG (2007) Liquid and magma viscosity in the Anorthite–Forsterite–Diopside–Quartz system, and implications for the viscosity–temperature paths of cooling magmas. J Geophys Res B 112:10203. doi:10.1029/2006JB004812

Höfer M, Schilling FR (2002) Heat transfer in quartz, orthoclase, and sanidine at elevated temperature. Phys Chem Miner 29:571–584

Hofmeister AM (2006) Thermal diffusivity of garnets at high temperature. Phys Chem Miner 33:45–62

Hofmeister AM (2007a) Dependence of thermal transport properties on pressure. Proc Natl Acad Sci 104:9192–9197. doi:10.1073/pnas.0610734104

Hofmeister AM (2007b) Thermal diffusivity of aluminous spinels and magnetite at elevated temperature with implications for heat transport in Earth's transition zone. Am Mineral (in press)

Hofmeister AM, Pertermann M (in review) Thermal diffusivity of clinopyroxenes at elevated temperature. Eur J Mineral

Hofmeister AM, Yuen DA (2007) The threshold dependencies of thermal conductivity and implications on mantle dynamics. J Geodyn 44:186–199

Hofmeister AM, Pertermann M, Branlund J, Whittington AG (2006) Geophysical implications of reduction in thermal conductivity due to hydration. Geophys Res Lett 33. doi:10.1029/2006GL026036

Hofmeister AM, Pertermann M, Branlund JM (2007) Thermal conductivity of the Earth. In: Schubert G (ed) Treatise in geophysics, vol 2. Mineral Physics (edited by G.D. Price) (Elsevier), Chap 18 (in press)

Hovis GL, Brennan S, Keohane M, Crelling J (1999) High-temperature X-ray investigation of sanidine-analbite crystalline solutions: thermal expansion, phase transitions, and volumes of mixing. Can Mineral 37:701–709

Jewell JM, Shaw CM, Shelby JE (1993) Effects of water contenton aluminosilicate glasses and the relation to strong/gragile liquid theory. J Noncryst Solids 152:32–41

Lange RA (2007) The density and compressibility of $KAlSi_3O_8$ liquid to 6.5 GPa. Am Mineral 92:114–123

Lee HL, Hasselman DPH (1985) Comparison of data for thermal diffusivity obtained by laser-flash method using thermocouple and photodector. J Am Ceram Soc 68:C12–C13

Lee DW, Kingery WD (1960) Radiation energy transfer and thermal conductivity of ceramic oxides. J Am Ceram Soc 43:594–607

Mehling H, Hautzinger G, Nilsson O, Fricke J, Hofmann R, Hahn O (1998) Thermal diffusivity of semitransparent materials determined by the laser-flash method applying a new mathematical model. Int J Thermophys 19:941–949

Mitra SS (1969) Infrared and Raman spectra due to lattice vibrations. In: Nudelman S, Mitra SS (eds) Optical properties of solids. Plenum, New York, p 333–452

Nye JF (1985) Physical properties of crystals: their representation by tensors and matrices. Clarendon, Oxford, 329 pp

Nyfeler D, Armbruster T, Villa IM (1998) Si, Al, Fe order–disorder in Fe-bearing K-feldspar from Madagascar and its implications to Ar diffusion. Schweiz Mineral Petrograph Mitt 78:11–20

Okamura S, Nakamura M, Nakashima S (2003) Determination of molar absorptivitiy of IR fundamental OH-stretching vibration in rhyolitic glasses. Am Mineral 88:1657–1662

Osako M, Ito E, Yoneda A (2004) Simultaneous measurements of thermal conductivity and thermal diffusivity for garnet and olivine under high pressure. Phys Earth Planet Inter 143, 144:311–320

Pertermann M, Hofmeister AM (2006) Thermal diffusivity of olivine-group minerals. Am Mineral 91:1747–1760

Richet P (1987) Heat capacity of silicate glasses. Chem Geol 62:111–124

Richet P, Bottinga Y (1984) Glass transition and thermodynamic properties of $SiO_2$, $NaAlSi_nO_{2n+2}$ and $KAlSi_3O_8$. Geochim Cosmochim Acta 48:453–470

Romano C, Hess KU, Mincione V, Poe B, Dingwell DB (2001) The viscosities of hydrous $XalSi_3O_8$ (X = Li, Na, K, $Ca_{0.5}$, $Mg_{0.5}$) melts. Chem Geol 174:115–132

Sass JH (1965) The thermal conductivity of fifteen feldspar specimens. J Geophys Res 70:4064–4065

Snyder D, Gier E, Carmichael I (1994) Experimental determination of the thermal conductivity of molten $CaMgSi_2O_6$ and the transport of heat through magmas. J Geophys Res 99:15503–15516

Stebbins JF, Carmichael ISE, Weill DE (1983) The high-temperature liquid and glass heat contents and heats of fusion of diopside, albite, sanidine, and nepheline. Am Mineral 68:717–730

Stebbins JF, Carmichael ISE, Moret LK (1984) Heat capacities and entropies of silicate liquids and glasses. Contrib Mineral Petrol 86:131–148

Stein D, Spera F (1994) Experimental rheometry of melts in system $NaAlSiO_4$–$SiO_2$: implications for melt structure and dynamics. Am Mineral 78:710–723

Stein DJ, Spera FJ (1998) New high-temeprature rotational rheometer for silicate melts, magmatic suspensions, and emulsions. Rev Sci Inst 69:3398–3402

Stein DJ, Spera FJ (2001) Shear viscosity of rhyolite-vapor emulsions at magmatic temperatures by concentric cylinder rheometry. J Volcanol Geotherm Res 113:243–258

Toplis MJ, Dingwell DB, Hess KU, Lenci T (1997) Viscosity, fragility, and configurational entropy of melts along the join $SiO_2$–$NaAlSiO_4$. Am Mineral 82:979–990

Urbain G, Bottinga Y, Richet P (1982) Viscosity of liquid silica, silicates and aluminosilicates. Geochim Cosmochim Acta 46:1061–1072

Whittington A, Richet P, Behrens H, Holtz F, Scaillet B (2004) Experimental temperature–X($H_2O$)–viscosity relationship for leucogranites, and comparison with synthetic silicic liquids. Trans R Soc Edinburgh Earth Sci 95:59–72

Zulumyan NO, Mirgorodskii AP, Pavinich VF, Lazarev AN (1976) Study of calculation of the vibrational spectrum of a crystal with complex polyatomic anion. Diopside $CaMgSi_2O_6$. Opt Spectrosc 41:622–627